

# Tailoring multilayer quantum wells for spintronic devices

S. Ullah,<sup>1</sup> G. M. Gusev,<sup>1</sup> A. K. Bakarov,<sup>2</sup> and F. G. G. Hernandez<sup>1,\*</sup>

<sup>1</sup>*Instituto de Física, Universidade de São Paulo,*

*Caixa Postal 66318 - CEP 05315-970, São Paulo, SP, Brazil*

<sup>2</sup>*Institute of Semiconductor Physics and Novosibirsk State University, Novosibirsk 630090, Russia*

(Dated: July 25, 2022)

We investigate long-lived spin coherence of a high mobility dense two-dimensional electron gas in multilayer GaAs quantum wells. The dynamics of the spin polarization was optically studied using pump-probe techniques: time-resolved Kerr rotation and resonant spin amplification. For samples doped beyond the metal-to-insulator transition, the tailoring of the spin-orbit interaction by the sample parameters of structural symmetry (Rashba constant), width and electron density (Dresselhaus linear and cubic constants) allows to attain long dephasing time in the few nanoseconds range in double and triple quantum wells. The determination of the scales: transport scattering time, single-electron scattering time, electron-electron scattering time, and the spin polarization decay time with and without magnetic field further supports the possibility of using n-doped multilayer systems for developing spintronic devices.

## I. INTRODUCTION

A milestone for practical applications of spintronic devices is a long-lasting spin coherence time ( $T_2^*$ ) for ensembles.<sup>1</sup> The tunability of  $T_2^*$  have been widely studied in semiconductor quantum wells (QWs) with a variety of optical techniques developed for the study of the spin polarization dynamics and the spin relaxation mechanisms.<sup>2-5</sup> For example, in n-type samples, it was observed that the doping level has a major role in attaining or limiting long coherence time with  $T_2^*$  changing from tens of picoseconds up to nanoseconds.<sup>6-9</sup> The turning point, where  $T_2^*$  decreases with an increase of the electron concentration, was found at the metal-to-insulator transition for bulk<sup>10,11</sup> ( $2 \times 10^{16} \text{ cm}^{-3}$ ) and GaAs QWs<sup>12</sup> ( $5 \times 10^{10} \text{ cm}^{-2}$ ). Beyond this point, the Dyakonov-Perel (DP) spin relaxation mechanism is dominant and controlled by electron-electron collisions.<sup>13</sup>

The DP mechanism defines a decay time, for the spin polarization along the QW out-of-plane direction, limited by the spin-orbit mechanisms giving the path to long-lived spin coherence. It can be calculated according to:  $t_z^{-1} = 8D_s m^2 \hbar^{-4} [\alpha^2 + (\beta_1 - \beta_3)^2 + \beta_3^2]$ , where  $D_s$  is the spin diffusion constant,  $\alpha$  is the Rashba coefficient due to structural inversion asymmetry, and  $\beta_1$  and  $\beta_3$  are the linear and cubic spin-orbit constants due to the Dresselhaus bulk inversion asymmetry.<sup>14,15</sup>

Recently, the authors demonstrated that multilayer QWs are exceptional platforms for the investigation of current-induced spin polarization effects.<sup>16,17</sup> While such complex systems also offer new possibilities for applications, for example in the production of spin blockers<sup>18</sup> and filters,<sup>19</sup> the study of long-living spin coherence in double (DQW) and triple quantum wells (TQW) is still required. Here, we report on the coherent spin dynamics in multilayer quantum wells using time-resolved Kerr rotation (TRKR) and resonant spin amplification (RSA). The sample structure allowed to control the DP mechanism by tailoring the spin-orbit constants through the well width, symmetry and subband concentration param-

eters. Remarkably, it results in coherence times in the nanoseconds range even for DQW and TQW samples with individual subband density beyond the metal-to-insulator transition.

## II. EXPERIMENT

We investigated two different samples, one double and one triple quantum well, both containing a dense two-dimensional electron gas (2DEG) with equal total density. The DQW sample consists of a wide symmetrically doped GaAs well with  $w = 45 \text{ nm}$ , total electron density  $n_t = 9.2 \times 10^{11} \text{ cm}^{-2}$  and mobility  $\mu = 1.9 \times 10^6 \text{ cm}^2/\text{Vs}$ . The electronic system forms a DQW configuration with symmetric and antisymmetric wave functions for the two lowest subbands with subband separation  $\Delta_{12} = 1.4 \text{ meV}$  and approximately equal subband density  $n_s$ .<sup>20</sup> Fig. 1(a) shows the calculated DQW band structure and the charge density for both subbands.

The second sample is a symmetrically doped GaAs TQW with 2 nm-thick  $\text{Al}_{0.3}\text{Ga}_{0.7}\text{As}$  barriers,  $n_t = 9 \times 10^{11} \text{ cm}^{-2}$  and  $\mu = 5 \times 10^5 \text{ cm}^2/\text{Vs}$ . The central well width is 22 nm and both side wells have equal widths of 10 nm. The central well has a larger width in order to be populated because the electron density tends to concentrate mostly in the side wells, as result of electron repulsion and confinement. The estimated density in the central well is 35% smaller than in the side wells. The coupling strength between the quantum wells is characterized by the separation energies  $\Delta_{ij}$  of the three occupied subbands ( $i, j = 1, 2, 3$ ) given by  $\Delta_{12} = 1.0 \text{ meV}$ ,  $\Delta_{23} = 2.4 \text{ meV}$ ,  $\Delta_{13} = 3.4 \text{ meV}$ .<sup>21</sup>

TRKR and RSA were used to probe the coherent spin dynamics of the electron gas. For optical excitation, we used a mode-locked Ti-sapphire laser with pulse duration of 100 fs and repetition rate of  $f_{rep} = 76 \text{ MHz}$  corresponding to a repetition period ( $t_{rep}$ ) of 13.2 ns. The time delay  $\Delta t$  between pump and probe pulses was varied by a mechanical delay line. The pump beam was cir-

cularly polarized by means of a photo-elastic modulator operated at a frequency of 50 kHz. The probe beam was not modulated, and the rotation of its polarization upon reflection was recorded as function of  $\Delta t$  and detected with a balanced bridge using coupled photodiodes. The laser wavelength was tuned to obtain the TRKR energy dependence in each sample. The samples were immersed in the variable temperature insert of a split-coil superconductor magnet in the Voigt geometry.

### III. RESULTS AND DISCUSSION

The time evolution of the spin dynamics for the DQW up to 2 T is demonstrated in Fig. 1(b) with pump/probe power of 1 mW/300  $\mu$ W. The TRKR oscillations are associated with the precession of coherently excited electron spins about the in-plane magnetic field. To obtain the spin coherence time, the evolution of the Kerr rotation angle can be described by an exponentially damped harmonic:

$$\theta_K(\Delta t) = A \exp(-\Delta t/T_2^*) \cos(\omega_L \Delta t + \phi) \quad (1)$$

where  $A$  is the initial spin polarization build-up by the pump,  $\phi$  is the oscillation phase, and  $\omega_L = g\mu_B B/\hbar$  is the Larmor frequency with magnetic field  $B$ , electron  $g$ -factor (absolute value)  $g$ , Bohr magneton  $\mu_B$ , and reduced Planck's constant  $\hbar$ . The magnetic field dependence of  $\omega_L$  and  $T_2^*$  are shown in Fig. 1(c) and (d). Solid lines are fits to the data. One can clearly see that the spin precession frequency increases with  $B$  following the linear dependence of the Larmor frequency on the applied field. The value of the fitted  $g$ -factor is 0.453 which is close to absolute value for bulk GaAs and similar to the value measured for a quase-two-dimensional system in a single barrier heterostructure with two-subbands occupied.<sup>22</sup>

According to the Dyakonov-Perel mechanism, the observed exponential decay at  $B = 0$  corresponds to the strong scattering regime.<sup>13,23</sup> In the opposite case, where the spin precess more than a revolution before being scattered, an oscillatory behavior would be expected. The measured value of the decay time for the spin polarization along the  $z$ -direction (out-of-plane) at zero external field is 1.1 ns. For our symmetric, wide and dense quantum well; we estimate  $\alpha \simeq 0$ ,  $\beta_1 = -\gamma(\pi/w)^2 = 0.49 \times 10^{-13} \text{ eVm}$ , and  $\beta_3 = -\frac{1}{2}\gamma\pi n_s = 0.70 \times 10^{-13} \text{ eVm}$  for the first subband using  $\gamma = -10 \text{ eV\AA}^3$ .<sup>24</sup> The charge diffusion constant can be estimated from the Fermi velocity  $v_F = \hbar\sqrt{2\pi n_s}/m$  and the transport scattering time  $\tau = \mu m/e = 70 \text{ ps}$ , using the effective mass  $m$  and the electron's charge  $e$ , by  $D_c = v_F^2 \tau / 2 = 3 \text{ m}^2/\text{s}$ . The spin diffusion constant is approximately two orders of magnitude smaller than the same constant for charge.<sup>14</sup> Scaling  $D_s = 100 \text{ to } 300 \text{ cm}^2/\text{s}$ , we obtain  $t_z \sim [8D_s m^2 \hbar^{-4} \beta_3^2]^{-1} = 1.1 \text{ to } 3.3 \text{ ns}$ . Thus, the data at  $B = 0$  agrees with a DP mechanism where the spin dynamics are dominated by the cubic Dresselhaus term. The cancellation of  $\alpha \simeq 0$  and  $\beta_1 - \beta_3 \simeq 0$  through the

sample parameters shows a practical path for long-lived spin coherence in highly doped QWs.

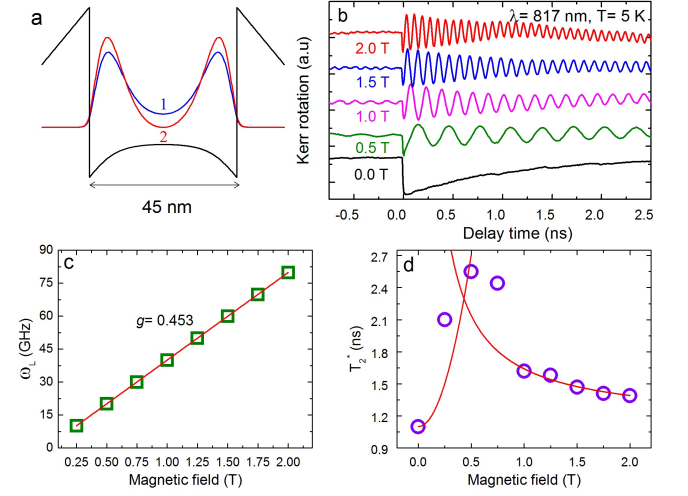


FIG. 1. (a) DQW band structure and the charge density for the first and second subbands. (b) KR as function of the pump-probe delay for different magnetic fields. (c) Larmor frequency  $\omega_L$  and (d)  $T_2^*$  fitted as function of  $B$ .

Increasing the magnetic field up to 0.5 T, the data yields a longer  $T_2^*$ . In this situation, the cyclotron motion acts as momentum scattering and leads to a less efficient spin relaxation in agreement with the DP model.<sup>25</sup> It is important to note that an in-plane magnetic field was applied using the Voigt configuration, it implies that the cyclotron motion is realized perpendicular to the QW plane and allowed due to the large QW width. The increase follows a quadratic dependence<sup>26</sup> with  $T_2^*(B)/T_2^*(0) = 1 + (\omega_c \tau_p^*)^2$  where  $\omega_c$  is the cyclotron frequency and  $\tau_p^*$  is the single-electron momentum scattering time. We found  $\tau_p^* = 0.92 \text{ ps}$  in agreement with the magnitude of the quantum lifetime measured by transport from the Dingle factor of the magneto-intersubband oscillations on the same sample.<sup>27</sup> The value for  $\tau_p^*$  is also in agreement with the determination of approximately 0.5 ps for QWs of shorter width.<sup>24</sup> One of the reasons for the large difference between  $\tau$  and  $\tau_p^*$  is the insensibility of the first to electron-electron scattering. The ratio of  $\tau/\tau_p^* \simeq 100$  implies that the dominant scattering from impurities is due to remote instead of background impurities.<sup>28</sup> If we consider that  $1/\tau_p^* = 1/\tau + 1/\tau_{ee}$ , we get a time scale of  $\tau_{ee} = \tau_p^*$  which demonstrates that electron-electron collisions dominate the microscopic scattering mechanisms as expected.<sup>13</sup>

Additionally, a further increase of the magnetic field leads to a faster oscillations decay due to the spread of the  $g$ -factor within the measured ensemble.<sup>29,30</sup> The size of the inhomogeneity  $\Delta g$  can be inferred by fitting the data according to  $1/T_2^*(B) = 1/T_2^*(0) + \Delta g \mu_B B / \sqrt{2}\hbar$  as shown in Fig. 1(d). From the  $1/B$  dependence,<sup>7,8</sup> we obtain  $\Delta g = 0.002$  or 0.44% and  $T_2^*(0) = 2 \text{ ns}$ .

The optical power influence on the time evolution of

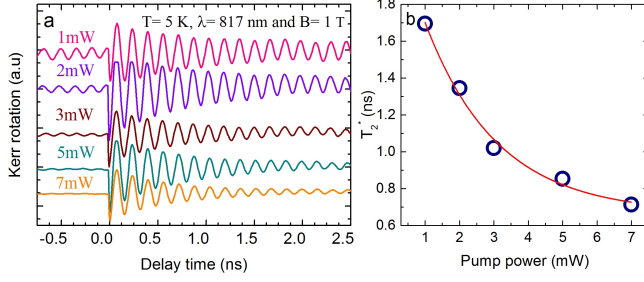


FIG. 2. (a) TRKR of the DQW as function of pump power and (b) the corresponding  $T_2^*$ .

the spin dynamics for the DQW sample are shown in Fig. 2(a) for 1 T. Only at low pump power, we observed negative delay oscillations of considerably large amplitude. The observation of electron spin polarization before the pump pulse arrival indicates that the spin polarization persists from the previous pump pulse, which took place  $t_{rep} = 13.2$  ns before. The excitation power dependence of  $T_2^*$  was plotted in Fig. 2(b) yielding an exponential decay. For single QW structures, the decreasing of the coherence time at high pump density was associated with the electrons delocalization caused by their heating due to the interaction with the photogenerated carriers.<sup>30</sup> A similar decrease was also attributed to an increased efficiency of the Bir-Aronov-Pikus mechanism induced by the larger hole photogenerated density in GaAs QWs.<sup>31</sup> However, it is unlikely to be relevant in our dense 2DEG where the photogenerated hole loses its spin and energy quickly and fastly recombines with an electron from the 2DEG. Nevertheless, as a key parameter for spin devices, we note that  $T_2^*$  remains near the nanoseconds range when the power is raised by almost one order of magnitude. At high excitation power, an additional short-living component in the signal becomes more significant. Upon the association of the 2DEG electrons dynamics with the long lasting oscillations, rather than with excitons or photo-excited electrons,<sup>30</sup> the use of a single exponential fitting mixes and underestimates  $T_2^*$ . In systems where  $T_2^*$  is comparable or longer than the laser repetition period, one can use the RSA technique to extract the spin dephasing time by scanning the magnetic field at a fixed pump-probe delay.<sup>7</sup>

Fig. 3(a) displays the RSA signals measured at different  $\Delta t$  with pump/probe power of 1 mW/300  $\mu$ W. We observed a series of sharp resonance peaks as a function of B corresponding to the electron spin precession frequencies which are commensurable with the pump pulse repetition period obeying the periodic condition:  $\Delta B = (\hbar f_{rep})/(g\mu_B)$ .<sup>7</sup> As function of the magnetic field, the RSA peaks amplitude decreases as result of the g-factor variation within the measured ensemble as commented. The RSA resonances are modulated by a slow oscillation that depends on  $f_d = 1/\Delta t$  according to the same periodic condition described above. Increasing the pump-probe delay causes the broadening of RSA peaks

corresponding to a shorten spin dephasing time.  $T_2^*$  can be directly evaluated from the width of the zero-field resonance using a Lorentzian model:<sup>7,17</sup>

$$\theta_K = A/[(\omega_L T_2^*)^2 + 1] \quad (2)$$

with half-width  $B_{1/2} = \hbar/(g\mu_B T_2^*)$ . The fitting result is displayed in Fig. 3(b) for negative and positive delays. The extracted values for  $T_2^*$  and for the amplitude are shown in Fig. 3(c) and (d) as function of  $\Delta t$ . For positive delays, both quantities display an exponential decay (solid line). However, the system coherence is recovered just before the pump arrival for the long-lived spin component in the system dynamics.<sup>32</sup> The RSA amplitude measured at negative delay was  $T_2^* = 4.4$  ns.

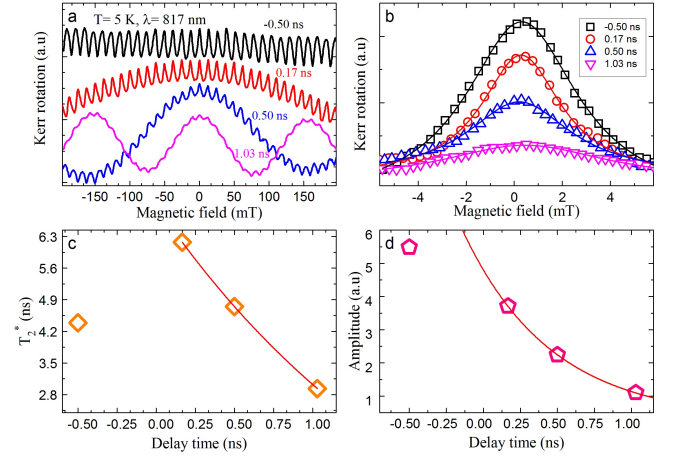


FIG. 3. (a) RSA scan of the DQW system obtained for different time delays. (b) Lorentzian fit of the zero-field resonance peak. (c)  $T_2^*$  and (d) Amplitude dependence on  $\Delta t$  from (b).

Concerning the subband dependence, the spin relaxation time was calculated to be identical in an electron system with two occupied subbands, although the higher subband may have a much larger inhomogeneous broadening, due to strong intersubband Coulomb scattering.<sup>22,33</sup> In our samples, we studied the pump/probe wavelength dependence as demonstrated in TRKR<sup>22</sup> and photoluminescence<sup>34,35</sup> studies of similar multilayer systems.

Figure 4(a) displays the RSA of the DQW sample for different pump-probe wavelengths at a fixed delay while scanning the external magnetic field. Panel 4(b) shows the comparison between the zero-field resonance peaks where the solid line is a Lorentzian fit to the data as described above.  $T_2^*$  and the amplitude obtained from (b) increase with the pump-probe wavelength as shown in Figures 4(c) and 4(d). Increasing the pump-probe energy about 3 meV ( $\simeq 2\Delta_{12}$ ), from 817 nm to 815 nm,  $T_2^*$  decreases less than 10% in Figure 4(d). In comparison, Figure 1 shows negative delay oscillations in the same wavelength range.<sup>36</sup> This small change could be associated with the relative similitude between the charge density distribution for both subbands. On the other

side, fast intersubband scattering may hide a difference in the spin-orbit interaction for the second subband as shown in recent calculations.<sup>37</sup>

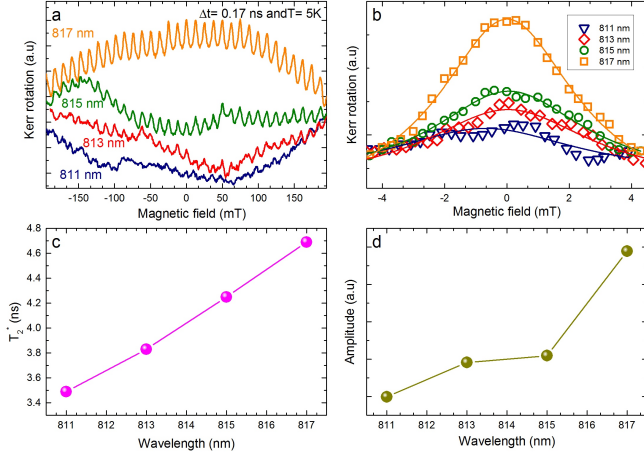


FIG. 4. (a) RSA scans of the DQW sample measured for different pump-probe wavelengths. (b) Fitting of the zero-field resonance. (c) Spin coherence time  $T_2^*$  and (d) Amplitude extracted from (b).

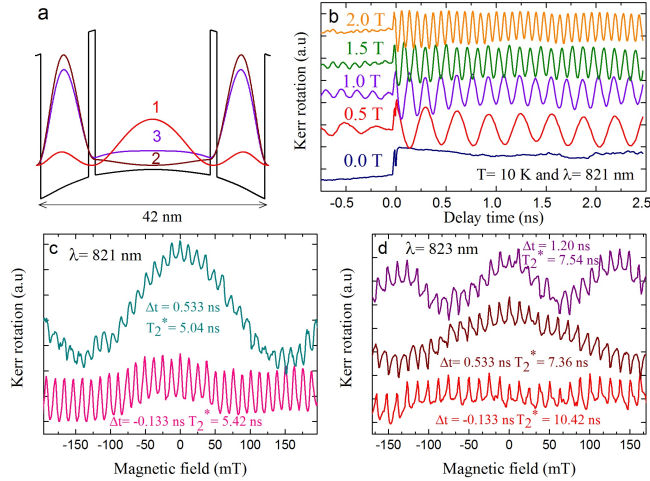


FIG. 5. (a) Band diagram and charge density for the TQW sample. (b) TRKR measured as function of the magnetic field. RSA scans of the TQW sample measured for different pump-probe delays with the corresponding extracted spin dephasing time at (c) 821 nm and (d) 823 nm.

Finally, we focus on the results for the TQW sample. Fig. 5(a) shows the calculated band diagram and charge density for three occupied subbands. The TRKR scans measured on the TQW sample as function of the magnetic field yield  $g = 0.452$ . Due to the long spin coher-

ence comparable with the laser repetition period, there is almost no decay over the measured time window (2.5 ns). In analogy to the DQW sample, we use the constructive interference of the coherence oscillations from successive pulses for extracting the spin coherence time by the RSA technique. Fig. 5(c) and (d) present the magnetic field scans of the KR amplitude performed at different pump/probe separation for 821 and 823 nm, respectively. From the Lorentzian fit of the zero-field peak, as for the DQW, the spin dephasing for the TQW sample was obtained revealing the longest  $T_2^* = 10.42$  ns at negative delay. In this case, the same energy increase ( $\sim 3$  meV  $\simeq \Delta_{13}$ ), leads to strong  $T_2^*$  decrease of almost 50%/30% at negative/positive delay. We note that, contrary to the DQW case, the first subband for the TQW have opposite charge distribution if compared with the higher subbands. While the first subband has the charge density more localized in the central well, the electrons in the second and third subbands are distributed in the side wells.

#### IV. CONCLUSIONS

In conclusion, we have studied the spin dynamics of a two-dimensional electron gas in multilayer QWs by TRKR and RSA. The dependence of spin dephasing time on the experimental parameters as magnetic field, pump power, and pump-probe delay was demonstrated. In the DQW sample,  $T_2^*$  extends to 4.4 ns at negative delay. Additionally, for the TQW sample,  $T_2^*$  exceeding 10 ns was observed. The results found are among the longest  $T_2^*$  reported for samples of similar doping level<sup>12,26</sup> and comparable with nominally undoped narrow GaAs QWs<sup>38</sup> and low density 2DEGs in CdTe QWs<sup>30</sup>. The measured long spin dephasing time was tailored by the control of the QW width, symmetry and electron density. The spin dynamics is dominated by the DP mechanism through the cubic Dresselhaus interaction. All the relevant time scales were determined indicating the importance of each scattering mechanisms in the spin dynamics. We demonstrate that the wave function engineering in multilayer QWs may and provide practical paths to control the dynamics in spintronic devices.

#### ACKNOWLEDGMENTS

F.G.G.H. acknowledge the financial support of this work by Grants No. 2009/15007-5, No. 2013/03450-7, and No. 2014/25981-7 São Paulo Research Foundation (FAPESP). S.U. gratefully acknowledge TWAS/CNPq for the financial support.

- 
- \* Corresponding author.  
Electronic address: felixggh@if.usp.br
- <sup>1</sup> M. W. Wu, J. H. Jiang, and M. Q. Weng, *J. Phys. Rep.* **493**, 61 (2010).
  - <sup>2</sup> E. A. Zhukov, D. R. Yakovlev, M. Bayer, G. Karczewski, T. Wojtowicz, and J. Kossut, *Physica Status Solidi (b)* **243**, 878 (2006).
  - <sup>3</sup> K. Biermann, A. Hernández-Mínguez, R. Hey, and P. V. Santos, *Journal of Applied Physics* **112**, 083913 (2012).
  - <sup>4</sup> V. Sih and D. D. Awschalom, *Journal of Applied Physics* **101**, 081710 (2007).
  - <sup>5</sup> M. Griesbeck, M. M. Glazov, E. Y. Sherman, D. Schuh, W. Wegscheider, C. Schuller, and T. Korn, *Phys. Rev. B* **85**, 085313 (2012).
  - <sup>6</sup> I. Y. Gerlovin, Y. P. Efimov, Y. K. Dolgikh, S. A. Eliseev, V. V. Ovsyankin, V. V. Petrov, R. V. Cherbunin, I. V. Ignatiev, I. A. Yugova, L. V. Fokina, et al., *Phys. Rev. B* **75**, 115330 (2007).
  - <sup>7</sup> J. M. Kikkawa and D. D. Awschalom, *Phys. Rev. Lett.* **80**, 4313 (1998).
  - <sup>8</sup> R. Bratschitsch, Z. Chen, S. T. Cundiff, E. A. Zhukov, D. R. Yakovlev, M. Bayer, G. Karczewski, T. Wojtowicz, and J. Kossut, *Appl. Phys. Lett.* **89**, 221113 (2006).
  - <sup>9</sup> L. V. Fokina, I. A. Yugova, D. R. Yakovlev, M. M. Glazov, I. A. Akimov, A. Greilich, D. Reuter, A. D. Wieck, and M. Bayer, *Phys. Rev. B* **81**, 195304 (2010).
  - <sup>10</sup> R. I. Dzhioev, K. V. Kavokin, V. L. Korenev, M. V. Lazarev, B. Y. Meltser, M. N. Stepanova, B. P. Zakharchenya, D. Gammon, and D. S. Katzer, *Phys. Rev. B* **66**, 245204 (2002).
  - <sup>11</sup> M. Römer, H. Bernien, G. Müller, D. Schuh, J. Hübner, and M. Oestreich, *Phys. Rev. B* **81**, 075216 (2010).
  - <sup>12</sup> J. S. Sandhu, A. P. Heberle, J. J. Baumberg, and J. R. A. Cleaver, *Phys. Rev. Lett.* **86**, 2150 (2001).
  - <sup>13</sup> W. J. H. Leyland, G. H. John, R. T. Harley, M. M. Glazov, E. L. Ivchenko, D. A. Ritchie, I. Farrer, A. J. Shields, and M. Henini, *Phys. Rev. B* **75**, 165309 (2007).
  - <sup>14</sup> M. P. Walser, C. Reichl, W. Wegscheider, and G. Salis, *Nature Physics* **8**, 757 (2012).
  - <sup>15</sup> J. Kainz, U. Rössler, and R. Winkler, *Phys. Rev. B* **70**, 195322 (2004).
  - <sup>16</sup> F. G. G. Hernandez, L. M. Nunes, G. M. Gusev, and A. K. Bakarov, *Phys. Rev. B* **88**, 161305(R) (2013).
  - <sup>17</sup> F. G. G. Hernandez, G. M. Gusev, and A. K. Bakarov, *Phys. Rev. B* **90**, 041302(R) (2014).
  - <sup>18</sup> S. Souma, A. Sawada, H. Chen, Y. Sekine, M. Eto, and T. Koga, *Phys. Rev. Applied* **4**, 034010 (2015).
  - <sup>19</sup> T. Koga, J. Nitta, H. Takayanagi, and S. Datta, *Phys. Rev. Lett.* **88**, 126601 (2002).
  - <sup>20</sup> S. Wiedmann, G. M. Gusev, O. E. Raichev, A. K. Bakarov, and J. C. Portal, *Phys. Rev. B* **84**, 165303 (2011).
  - <sup>21</sup> S. Wiedmann, N. C. Mamani, G. M. Gusev, O. E. Raichev, A. K. Bakarov, and J. C. Portal, *Phys. Rev. B* **80**, 245306 (2009).
  - <sup>22</sup> F. Zhang, H. Z. Zheng, Y. Ji, J. Liu, and G. R. Li, *Europhys. Lett.* **83**, 47007 (2008).
  - <sup>23</sup> M. A. Brand, A. Malinowski, O. Z. Karimov, P. A. Marsden, R. T. Harley, A. J. Shields, D. Sanvitto, D. A. Ritchie, and M. Y. Simmons, *Phys. Rev. Lett.* **89**, 236601 (2002).
  - <sup>24</sup> M. P. Walser, U. Siegenthaler, V. Lechner, D. Schuh, S. D. Ganichev, W. Wegscheider, and G. Salis, *Phys. Rev. B* **86**, 195309 (2012).
  - <sup>25</sup> M. Griesbeck, M. M. Glazov, T. Korn, E. Y. Sherman, D. Waller, C. Reichl, D. Schuh, W. Wegscheider, and C. Schüller, *Phys. Rev. B* **80**, 241314(R) (2009).
  - <sup>26</sup> A. V. Larionov and A. S. Zhuravlev, *JETP Letters* **97**, 137 (2013).
  - <sup>27</sup> S. Wiedmann, G. M. Gusev, O. E. Raichev, A. K. Bakarov, and J. C. Portal, *Phys. Rev. Lett.* **105**, 026804 (2010).
  - <sup>28</sup> S. J. MacLeod, K. Chan, T. P. Martin, A. R. Hamilton, A. See, A. P. Micolich, M. Aagesen, and P. E. Lindelof, *Phys. Rev. B* **80**, 035310 (2009).
  - <sup>29</sup> A. Greilich, R. Oulton, E. A. Zhukov, I. A. Yugova, D. R. Yakovlev, M. Bayer, A. Shabaev, A. L. Efros, I. A. Merkulov, V. Stavarache, et al., *Phys. Rev. Lett.* **96**, 227401 (2006).
  - <sup>30</sup> E. A. Zhukov, D. R. Yakovlev, M. Bayer, M. M. Glazov, E. L. Ivchenko, G. Karczewski, T. Wojtowicz, and J. Kossut, *Phys. Rev. B* **76**, 205310 (2007).
  - <sup>31</sup> G. Wang, A. Balocchi, A. V. Poshakinskiy, C. R. Zhu, S. A. Tarasenko, T. Amand, B. L. Liu, and X. Marie, *New J. Phys.* **16**, 045008 (2014).
  - <sup>32</sup> I. A. Yugova, M. M. Glazov, D. R. Yakovlev, A. A. Sokolova, and M. Bayer, *Phys. Rev. B* **85**, 125304 (2012).
  - <sup>33</sup> M. Q. Weng and M. W. Wu, *Phys. Rev. B* **70**, 195318 (2004).
  - <sup>34</sup> Y. A. Pusep, L. F. dos Santos, G. M. Gusev, D. Smirnov, and A. K. Bakarov, *Phys. Rev. Lett.* **109**, 046802 (2012).
  - <sup>35</sup> L. F. dos Santos, B. G. Barbosa, G. M. Gusev, J. Ludwig, D. Smirnov, A. K. Bakarov, and Y. A. Pusep, *Phys. Rev. B* **89**, 195113 (2014).
  - <sup>36</sup> See Supplemental Material for more data on the signal wavelength dependence.
  - <sup>37</sup> J. Y. Fu and J. C. Egues, *Phys. Rev. B* **91**, 075408 (2015).
  - <sup>38</sup> R. I. Dzhioev, V. L. Korenev, B. P. Zakharchenya, D. Gammon, A. S. Bracker, J. G. Tischler, and D. S. Katzer, *Phys. Rev. B* **66**, 153409 (2002).